ARGONNE
NATIONAL
LABORATORY

INTRA-LABORATORY MEMO

November 10, 2000

TO: J. E. Herceg

FROM: T. H. Bauer

SUBJECT: A Preliminary Thermal and Hydraulic Assessment of the NuMi Shielding Design

REFERENCES

1. Cat James MARS calculations, private communication (from Dave Pushka), January, 2000.

2. SINDA/G (ver. 1.9), Network Analysis Inc., Tempe, AZ (1999).

3. F. Kreith and M. S. Bohn, *Principles of Heat Transfer, 4th Ed.*, Harper and Row Inc., New York, 1986.

Overview

The need to assess heat removal capability early in the design process arises from the large amounts of energy from the beam deposited as heat in a relatively thin layer of the thick steel shielding surrounding the chase. In accordance with requirements, principal concerns are maintaining acceptably low temperatures in the shielding, including both the enclosed interior chase region, itself, as well as shielding exterior surfaces. Since energy deposition is not spatially uniform, the potential for local hot spots must be addressed. Globally, any proposed cooling system in a near-adiabatic subterranean environment must also minimize heat leakage to the cave wall boundaries; *i.e.* efficiently scavenge and relocate all added heat (for ultimate removal by an HVAC system). Heat losses to cave wall boundaries must also be limited to prevent undesirable heatup (and expansion) of structural concrete.

This memo explores the engineering feasibility of heat removal from the beam chase and surrounding steel shielding by high-speed, high-volume flowing air. The basic concept is that chilled air flows down the cave through channels surrounding the steel shielding and returns through the beam chase. Based on the current steel and concrete shielding design configuration, rough scoping thermal and hydraulic calculations were made for (1) the pressure drop and power requirements to maintain high speed, high volume flow, (2) temperature rise in the bulk flowing air, and (3) temperature rises between the bulk air and the steel surface. The scoping analyses were used to determine a promising range of parameters and conditions and were followed by detailed 3D thermal analyses of actual shielding designs. Several iterations of detailed thermal performance analyses contributed to the development of the current shielding design.

To date, the principal conclusions of these analyses are:

1. High-volume air flow (~50,000 scfm) keeps bulk air temperature rise minimal (~3.5 C for 100 kW heat load) and can remove >95% of deposited heat.

2. High-speed air flow in chase (~48 fps) keeps the temperature rise at the steel surface reasonable (calc. ÄT's. 45 C).

3. Large cross sections available in chase and shielding periphery keep pressure drops and power requirements reasonable. (~2 in. H_2O and ~20 HP to drive flow through channels)

4. Peripheral flow outside the steel keeps structural concrete cool (calc. ÄT's~1 C).

5. There is persistent concern of high shielding block temperatures above the chase leading to possible misalignment of the first horn. Additional analysis is needed. Additional cooling and/or mechanical compensation may be required

6. In the event of continued heating following inadvertent loss of air flow, heatup to unacceptable levels requires many hours.

Heat Source

The fundamental heat source is radiation produced by interactions of high energy particles with the target and "horns" positioned in the chase. A 3-dimensional distribution of heat energy deposition in the steel surrounding the chase was calculated by Monte Carlo methods by Fermilab for representative beam operation [1]. Figures 1-3 show these calculated results (appropriately summed and averaged) to yield spatial distributions of heat deposition: down a 35 m length of the chase (Fig. 1, Z-dimension), along the side of the chase (Fig. 2, Y-dimension), and penetration into the shielding, itself (Fig. 3). Prominent peaks in Fig. 1 appear just downstream of assumed "horn" locations. Similarly the peak in the Fig. 2 distribution corresponds to the assumed location of the "horn" within the chase.

Because heat energy deposition in the shielding above and below the chase was not directly calculated in the Ref. 1 analysis, a simple scheme plausibly extrapolated Ref. 1 calculated values along the side to corresponding locations above and below the assumed position of a horn. Extrapolations to "above" and "below" locations also assumed approximate scaling factors inversely proportional to the distance between the horn and the particular shielding surfaces. This method results in ~62% of the total energy deposited on the sides of the chase (as directly calculated) with ~38% on the top and bottom (by extrapolation). The aggregate extrapolated energy deposition over the entire chase is 99.4 or ~100 kW.

A Scoping Analysis of Cooling with High-Speed Flowing Air

Table I Geometry Assumed in Hydraulic Analyses		
Region	Area (cm^2)	Hydraulic Diameter (cm)
Chase	$1.62x10^4$	86.6
Side Channel	$1.17x10^4$	25.4
Bottom Channel	$3.10x10^3$	18.5

The large open cross sections enclosed by the chase and between the steel and concrete shielding are potential flow channels for high-speed, high-volume flowing air. A brief scoping analysis indicates that a cooling approach in which chilled air flows down the cave around the periphery of the steel shielding and returns up the chase shows considerable promise.

For high volume air flow, bulk temperature rise is very small. For example, removing 100 kW with an air flow of 50,000 scfm (where the heat capacity of air is ~1 J/g-C and1 scfm = 0.57 g/s) leads to a bulk air temperature rise of only ~3.5 C. However, taking realistic account of wall heat transfer coefficients assures that the most significant temperature rises actually occur on the shielding surfaces inside the chase. Even here, wall temperatures are likely to be acceptable (i.e., below 100 C).

For the above 50,000 scfm airflow, nominal chase dimensions (including obstructions) imply an air velocity ~1800 cm/s and a wall heat transfer coefficient ~ $3.6x10^{-3}$ W/cm^2-C. We assume all heat is deposited directly on the chase surface. Using the flowing air to completely remove the maximum deposited heat flux, (calculated in Ref. 1 to be ~0.25 W/cm^2), we calculate a "hot spot" temperature rise on the chase wall of ~70 deg-C (above that of the air). It is important to note that this estimated temperature rise is extremely conservative and takes no credit for heat transfer in the shielding. More realistic temperature rise estimates taking account of these effects are considerably lower (see below).

Figure 4 presents estimated hydraulic characteristics for one possible cooling concept over a wide range of air flowrates. A full 52 m chase is included for conservatism (whereas heating was computed over only a 35 m length [1]). Geometry of the flow channel cross sections found in the present design is provided in Table I. Figure 4 shows calculations where no airflow is assumed in the "Top Channel" above the steel shielding and where the pressure drops in side and bottom channels are equal. These assumptions imply a mass flow split of ~83% and 17 % between the side and bottom channels, respectively. While it is clear that all hydraulic losses have not been considered, computed pressure drops and power requirements for total airflow in the neighborhood of 50,000 scfm are small enough to be practically achievable.

A Detailed Thermal Analysis

The above scoping calculations were followed by more detailed 3D thermal analyses using the network analysis code, SINDA/G [2]. SINDA/G models general networks of lumped parameter nodes interconnected by any desired conduction, convection, and radiation heat transfer paths. Fundamentally, SINDA/G's thermal network approach is highly "modular" and results in thermal models that can be adapted with relative efficiency to actual or proposed design changes.

(Network nodes may either contain heat capacity or represent surfaces. A number of solution-method options allow for accurate steady-state and transient solutions that balance energy globally and locally. An extensive library of options useful for heat transfer modeling and problem control are available. Also, user-supplied code for modeling and problem control is both straightforward and convenient.)

The 3D thermal model includes a 35 m long representation of the NuMi chase. Idealized X-Y cross sections and nodalization of the current shielding design are shown in Fig. 5. All dimensions shown are in cm. The cross section of the chase and immediately surrounding nodes were intentionally dimensioned to conform with the energy deposition model of Ref. 1. (We note that the chase dimensions in the present shielding design have changed somewhat. However, these differences are not expected to be of significance to thermal issues.) Away from the chase, X-Y plane nodes were enlarged up to roughly the size of shielding block dimensions. Bulk structural concrete is included in the model between the shielding and bounding rock surfaces. (A concrete surface forms each air channel's outer boundary.) The two air gaps indicated in the Fig. 5 cross sections model reflect two prominent gaps between shielding blocks actually present in the current shielding design.

Node size in the Z-direction also conforms to Ref. 1. The full 35 m of shielding is modeled as a stack of 1 m thick sections in good thermal contact.

To span a range of designs, two versions of the model have been used in these analyses (Figs. 5a and 5b) depending on whether cooling above the steel shielding blocks is passive (natural convection) or active (forced airflow).

Both versions assume specified flowrates of high-speed cooling air are input through air gaps surrounding the steel shielding. The temperature of the input cooling air is one boundary condition of these models. In the Fig. 5a version, airflow is forced only past side and bottom surfaces. In the Fig. 5b version, specified airflow is forced over the top surface as well. In both cases, all peripheral forced air flow streams recombine at the "downstream" Z-end of the model (35 m) and return back "upstream" through the chase. Hydraulic dimensions are those given in Table I. Convection heat transfer coefficients in the chase and peripheral channels were calculated using the forced-air Dittus-Boelter correlation [3]. In addition to forced convection, direct radiation heat transfer is computed between facing steel and concrete surfaces across each flow channel. The thickness of the

bulk concrete shielding surrounding the flow channels is included in the model. The "rock" labeled at the outer surfaces of the concrete represents a fixed temperature boundary of the model.

The Fig. 5a model assumes the top surface of the steel shielding is exposed to "stagnant" air at an assumed fixed temperature boundary. Heat transfer to this boundary is modeled as radiation and upward free convection from a heated surface (Fujii-Imura correlation [3]). In the Fig. 5b model, the "rock" boundary surface labeled above the top concrete surface simplifies a possibly more complex configuration and air gap. In both models, top surface simplifications are justified on the basis of the small heat flux expected through this surface.

In this study, all boundary temperatures were assumed to be 20-deg C.

Calculations

Results of some illustrative baseline steady-state and transient thermal analyses are shown in Figs. 6-15. Energy deposition was assumed to be as calculated in Ref. 1, extrapolated to include the entire chase. Total forced airflow is nominally assumed to be 50,000 scfm. Air above the steel shielding is assumed stagnant or a specified fraction of the total forced flow. Forced airflow split between side and bottom channels is the same 83% to 17% mass as assumed in the scoping analyses. Thermal conductivity of the steel shielding was assumed to be that of carbon steel. Apart from the air gaps indicated in Fig. 5, shielding blocks were assumed in good thermal contact.
In addition to the baseline described above, calculations were also performed for a range of input air flowrates. Also, to determine sensitivity to uncertain thermal conductivity and the possibility of poor thermal contact between shielding blocks, alternative calculations were also performed assuming stainless steel thermal conductivity, a factor of ~4-5 lower than carbon steel. Selected results from this wider range of conditions are found in Excel spreadsheets referenced in Appendix A.

Typical material and thermal properties assumed in these analyses are shown in Table II.

Discussion of Results

Figure 6a shows representative steady-state peak shielding temperatures computed down the chase

Table II Key Thermal Properties

Material	Density (g/cm^3)	Specific Heat (J/g-C)	Thermal Cond. (W/cm-C)	Emissivity
Carbon Steel	7.85	0.43	0.60	0.7
Stainless Steel	7.89	0.51	0.13	0.7
Concrete	2.09	0.84	0.012	0.8

(Z-dependence) in the case of stagnant air above the shielding. Figure 6b shows corresponding computed temperatures of flowing air and concrete. Figures 7a and 7b show the same temperatures computed with 50% of the airflow above the chase. In Figs. 6a and 7a, we note the sharp temperature peak evident at the hottest Z-node (Fig. 1) just downstream of the first horn. Figures 8-11 illustrate X and Y dependence of computed steady-state shielding temperatures computed at this Z-peak for the two cases shown in Figs 6 and 7. (See Fig. 5 for X and Y locations.) For these baseline cases, it is evident that computed temperatures in the steel shielding and bulk concrete generally meet design requirements by a comfortable margin. Also, Figures 6b and 7b show both the expected small global temperature rise in the flowing air and a very small rise in bulk structural concrete.

Computations shown in Figs. 12 and 13 assess the ability of the air cooling system to efficiently "scavenge" deposited heat and direct it through various heat removal pathways. For the case of stagnant air above the shielding, Fig. 12 shows dependence on total air flowrate (10,000-50,000 scfm). For the case of forced airflow above the shielding, Fig. 13 shows dependence on the fraction of airflow directed above the shielding for the baseline 50,000 scfm total flowrate. For the baseline 50,000 scfm cases we estimate a heat leakage to the rock wall of ~5% where the air above the shielding is stagnant and <2% in all computed cases where the airflow was forced. In both Fig. 12 and 13 examples, ~50% of deposited energy is removed directly from the chase with the remainder removed from locations along the shielding periphery.

Unlike the conservative assumption made in the scoping analysis, it is evident that heat transfer within and among the shielding blocks is quite important. A variety of parameters including: input flowrate, block thermal conductivity, locations of air gaps between blocks influence the relative importance of each shielding surface location in heat removal.

It is evident that lowering input flowrate will generally increase temperature, and as total flowrates are lowered toward 10,000 scfm computed temperature rise in the chase and the shielding blocks directly above the chase approach unacceptable levels (Appendix A and below). We note from Fig. 12 that reducing inlet flowrate also reduces the heat fraction removed in the chase.

The air gap next to the T-block (directly above the chase) leads to relatively high temperatures computed in the T-block (Figs. 8 and 9). Likewise, the air gap on the side of the chase reduces the heat removal fractions from the side (Figs. 8 - 11). Assumption of low (stainless-steel) thermal conductivity for the shielding blocks leads to (1) higher temperatures in the chase region, (2) lower heat removal fractions on the side and bottom, and (3) reduced importance of the assumed air gaps (Appendix A). Lowering thermal conductivity or adding air gaps tend to redistribute or skew high temperatures toward the chase.

In general, results show that the computed temperature field is relatively insensitive to the presence of forced or stagnant cooling air on top of the steel shielding (with total forced airflow fixed). Significant

changes are computed only around the shielding periphery. With forced airflow, temperatures at the top are somewhat lower. Temperatures on the sides and bottom are slightly higher.

There is some persistent concern of shielding block temperatures above the chase at the sharp temperature peak just downstream of the first horn. Overheating the nearby structure supporting the horn could lead to excessive thermal expansion and possible misalignment. In the baseline case shown for stagnant air cooling of the shielding top surface, the computed peak temperature at the top surface ~43 C is at best marginally acceptable. Lowering this temperature is clearly one motivation for introducing forced airflow at this location. However, the computed effect is not dramatic. Corresponding baseline computations where 50% of the forced airflow is directed above the steel lowers this computed temperature only by ~6 C. (With regard to other parametric variation, lowering air flowrate would raise this temperature. Lowering thermal conductivity would also lower it. Also, the average surface temperature of the shielding top is likely lower than the peak value directly above the chase- Figs 8 and 9.) Clearly additional thermal analysis of the module support structure region in concert with nearby shielding is needed. If such analyses indicate a need, additional active cooling or mechanical compensation (perhaps only at the Z-peak location) could be introduced.

Finally, for a rough preliminary assessment of temperature sensitivity to accidental and sudden loss of forced airflow, Figs. 14 and 15 show computed results of a transient heatup following a hypothetical sudden loss of all forced airflow and continuing energy deposition. Initial temperatures were baseline steady-state conditions. (Modeling assumptions included stagnant air above steel shielding and the same 20 C boundary temperature at the rock surface. Surface-to-air heat transfer correlations in the flow channels revert to correlations appropriate to laminar or stagnant flow.)

Basically, Figs. 14 and 15 update temperatures reported in Figs. 6a and 6b 24 hours after airflow terminates. Computed increases of selected temperatures over this time period are indicated. It is clear from the results shown that heatup of steel and concrete is extremely slow. Many hours would be required to generally raise temperatures to unacceptable levels. The air-cooling concept allows a wide safety margin for equipment repair and/or replacement.

DISTRIBUTION
K. Anderson, FNAL
H. J. Haupt, RAE
J. Hylen, FNAL
S. A. Kamal, RAE
L. Krajtl, TD
D. Pushka, FNAL
J. G. Saiveau, RAE

Fig. 1 Z-Dependence of Input Power

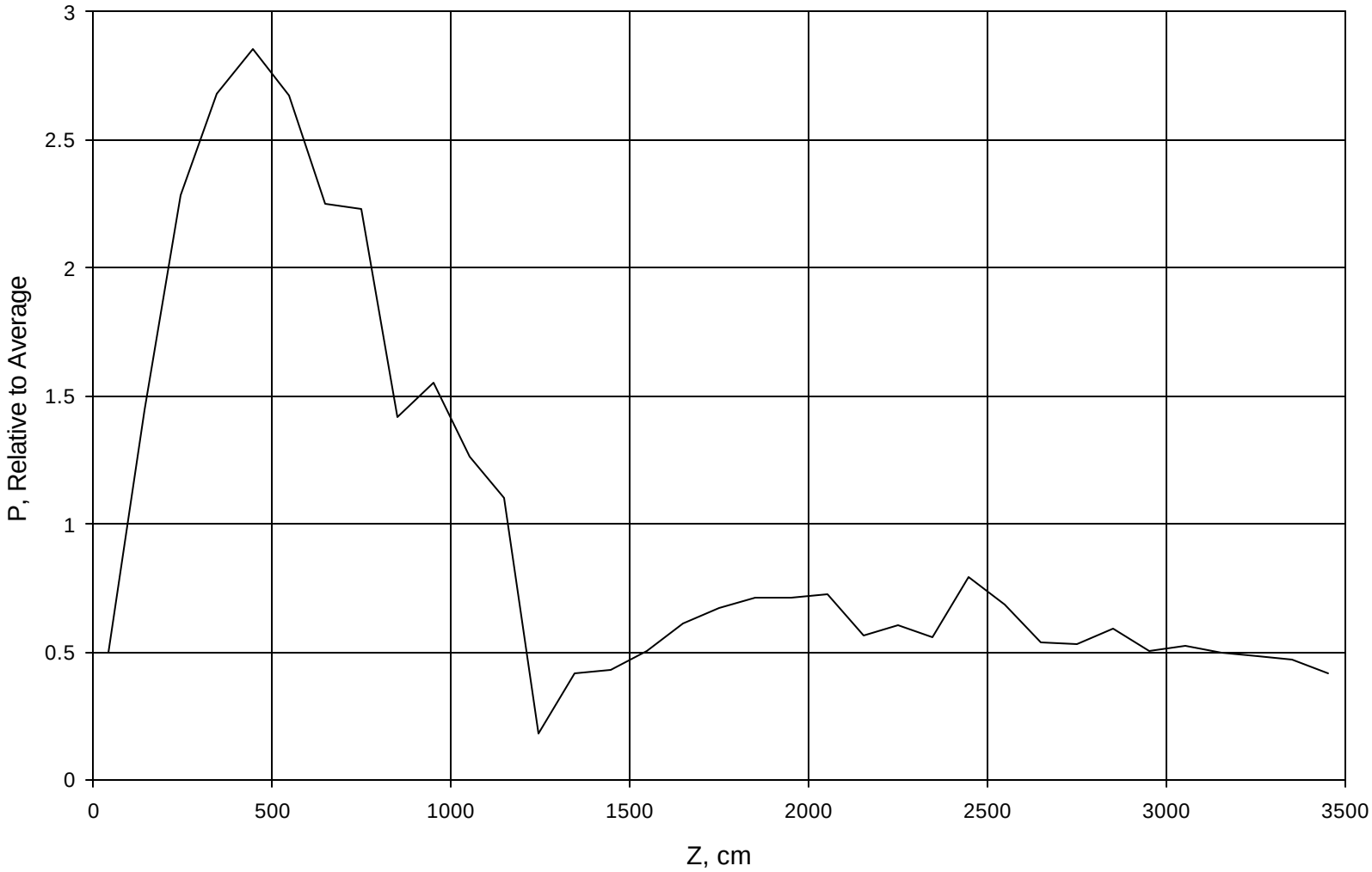

Fig. 2 Average Y-Dependence of Input Power Along Side of Chase

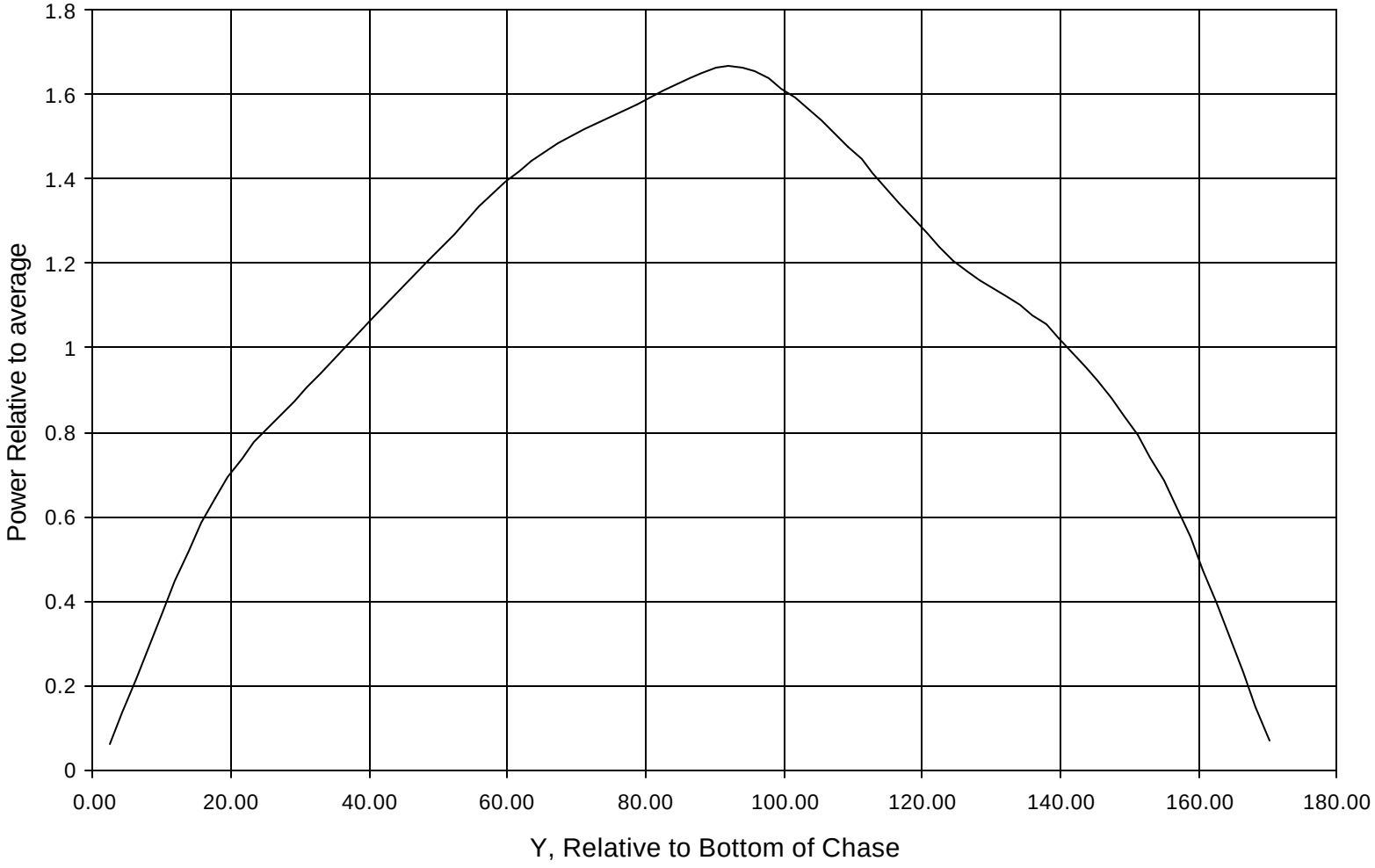

Fig. 3 Averaged Thermal Power Penetration into the Shielding

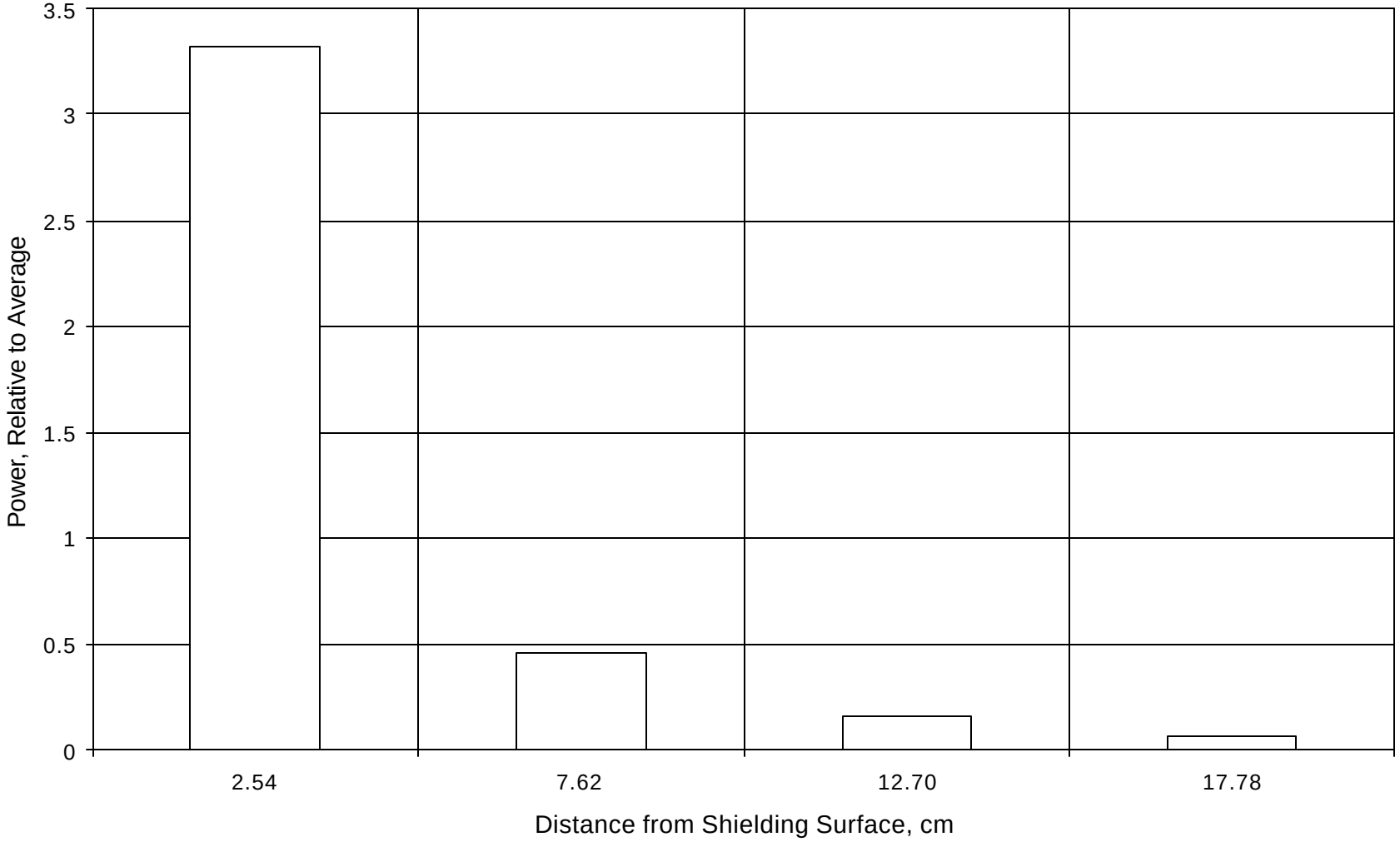

Fig. 4 Estimate of Cave Hydraulic Characteristics Versus Flowrate (Whole Chase)

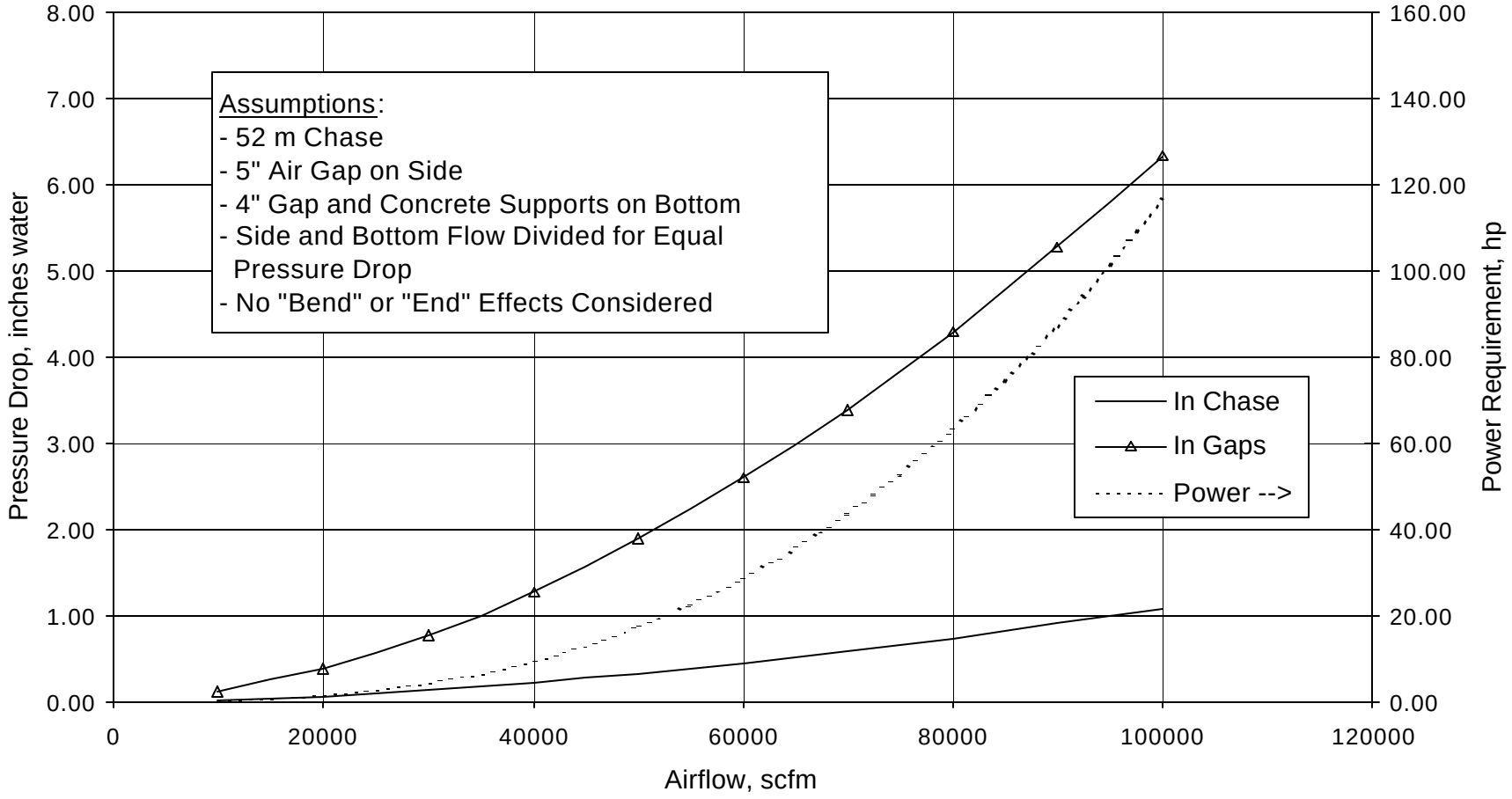

Fig. 5 X-Y Cross Section of the NUMI Shielding Thermal Model

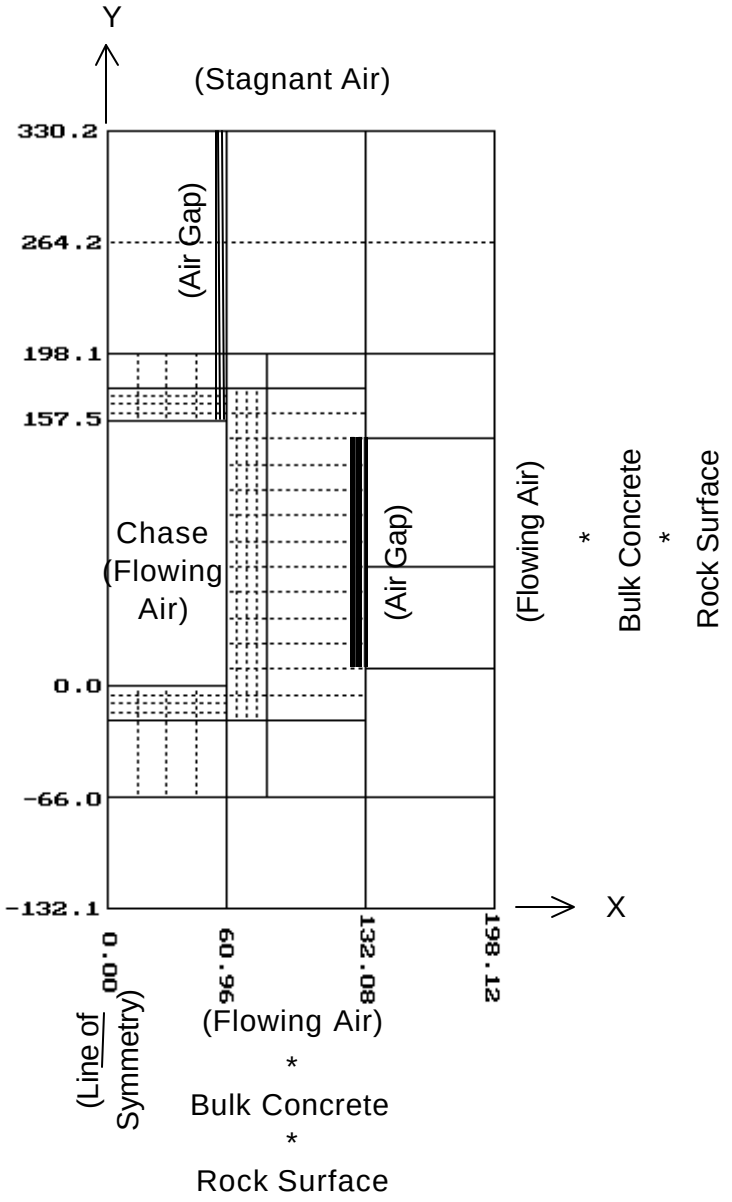

a. Stagnant Air Assumed Above Shielding

Fig. 5 (Cont.) X-Y Cross Section of the NUMI Shielding Thermal Model

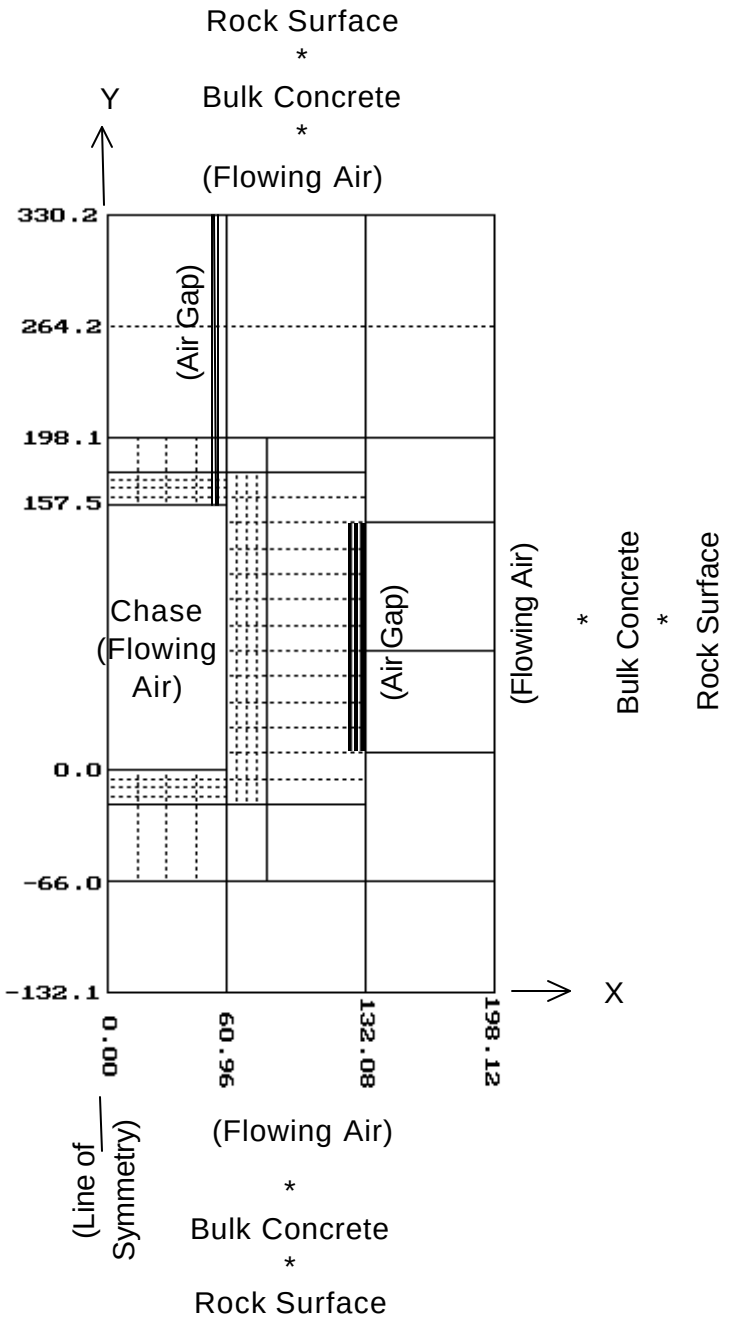

b. Flowing Air Assumed Above Shielding

Fig. 6a Computed Shielding Temperatures Down the Chase
(Stagnant Air Above Shielding)

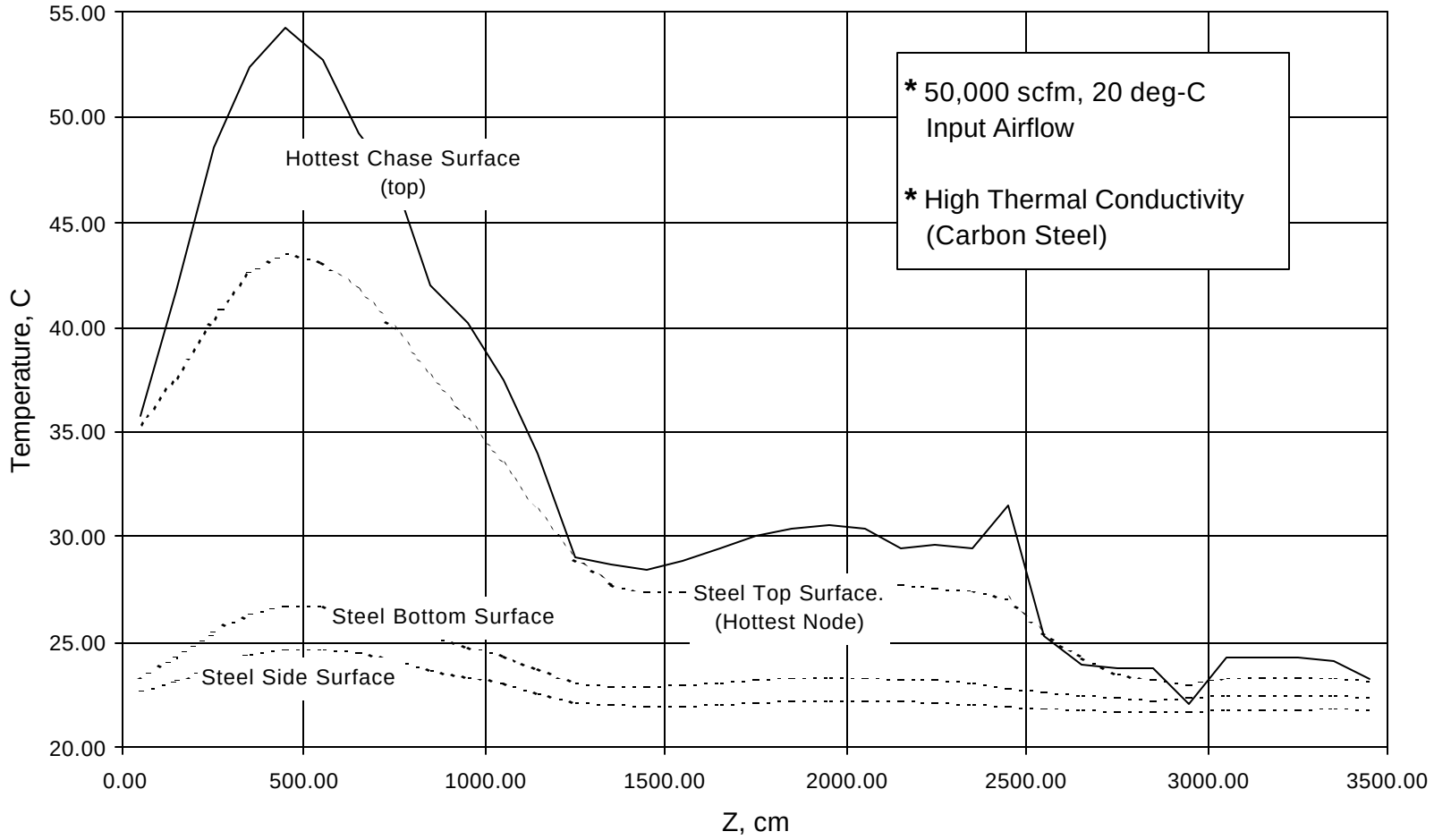

Fig. 6b Computed Air and ConcreteTemperatures Down the Chase
(Stagnant Air Above Shielding)

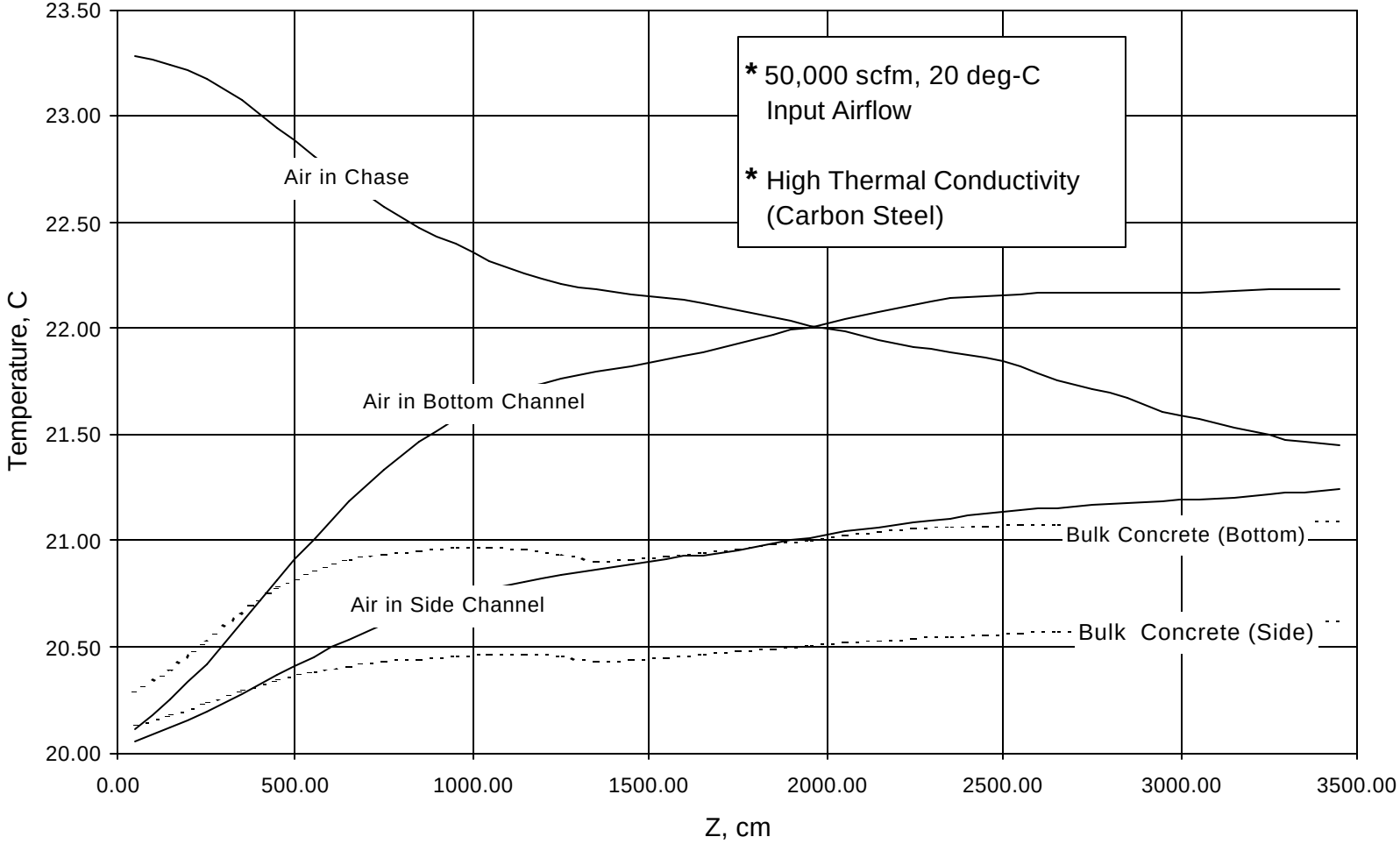

Fig. 7a Computed Shielding Temperatures Down the Chase
50% of Airflow on Top

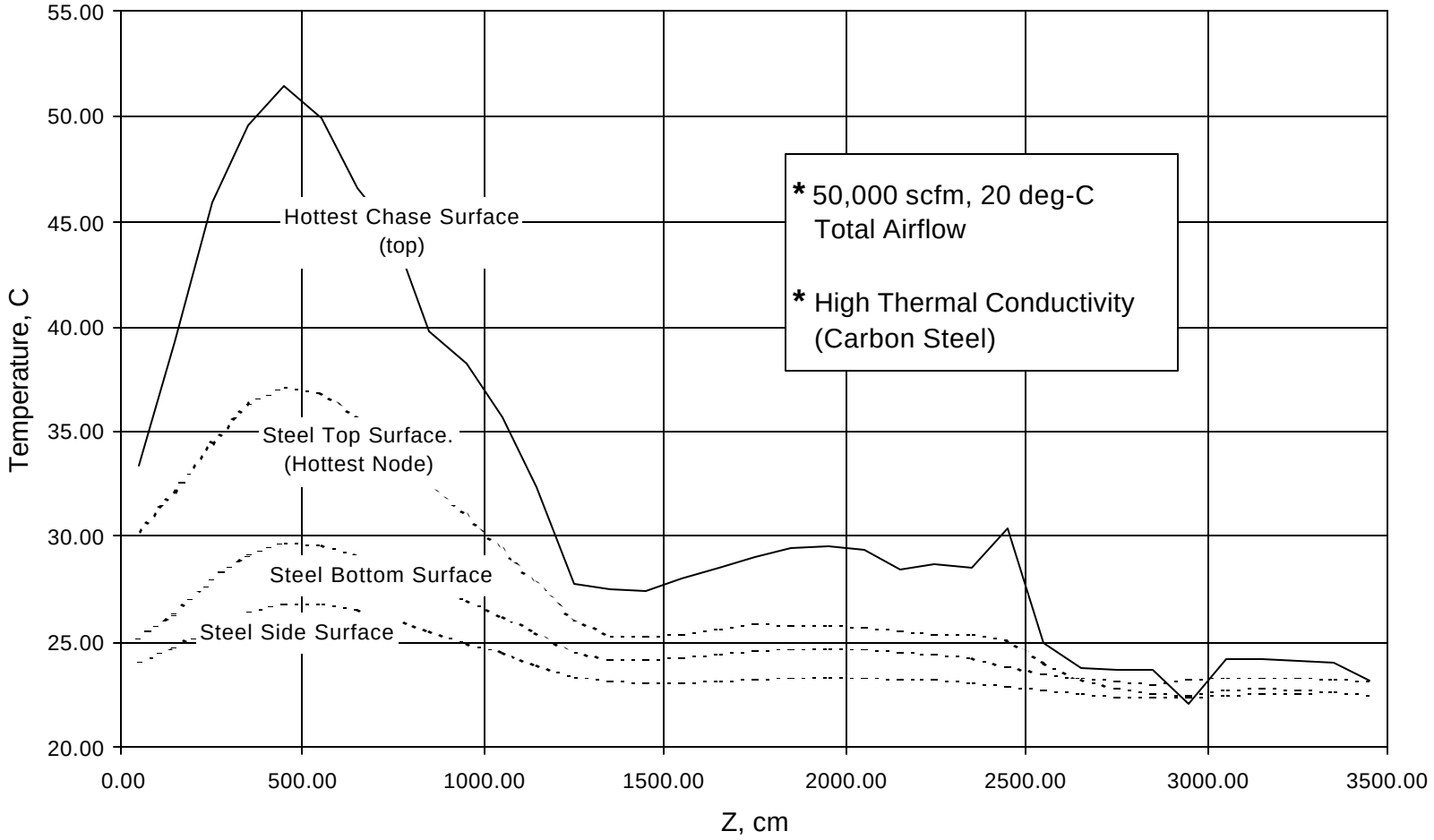

Fig. 7b Computed Air and ConcreteTemperatures Down the Chase
50% of Airflow on Top

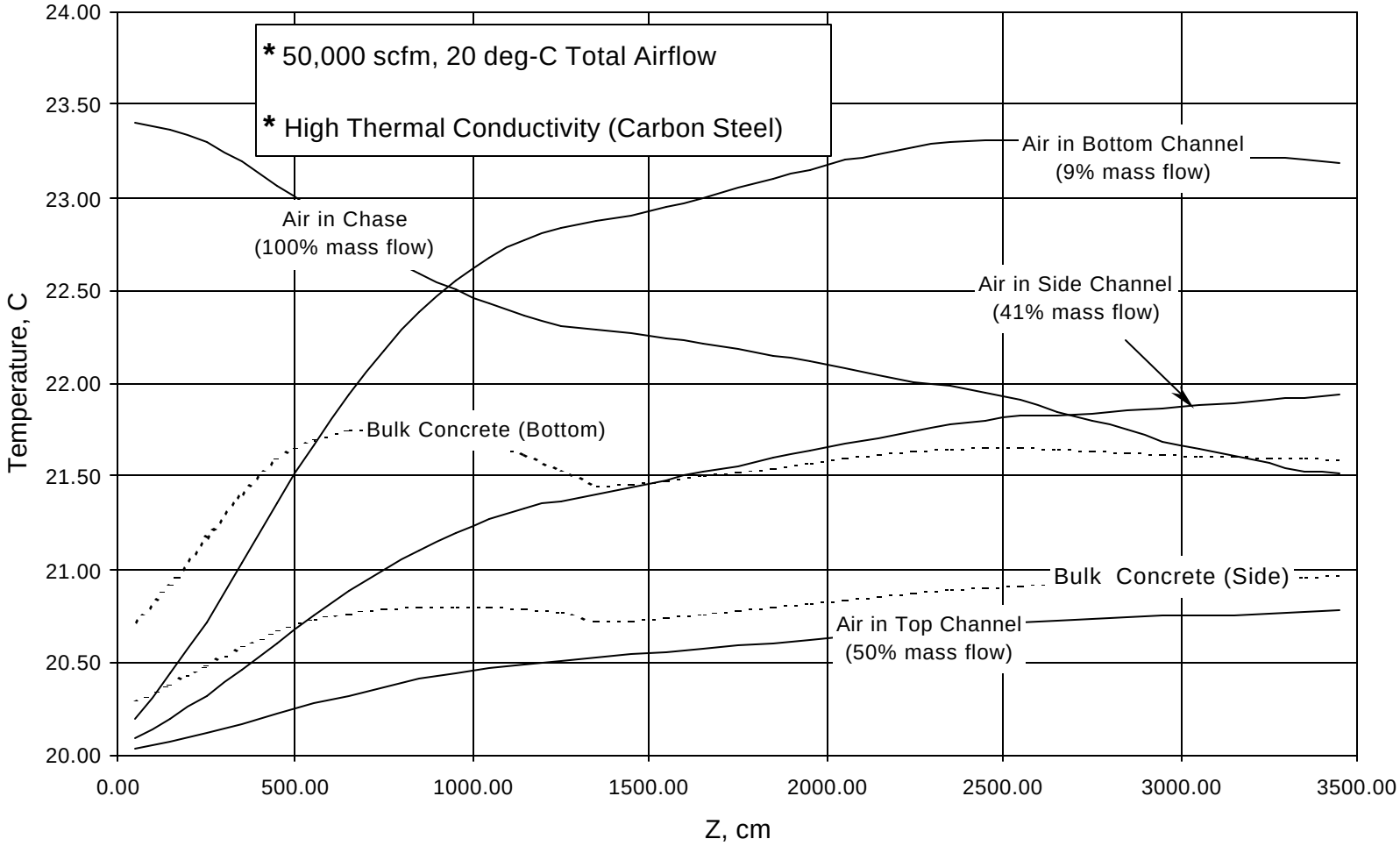

Fig. 8 Computed X-Dependence of Z-Peak (450 cm) Temperatures
(Stagnant Air Above Shielding)

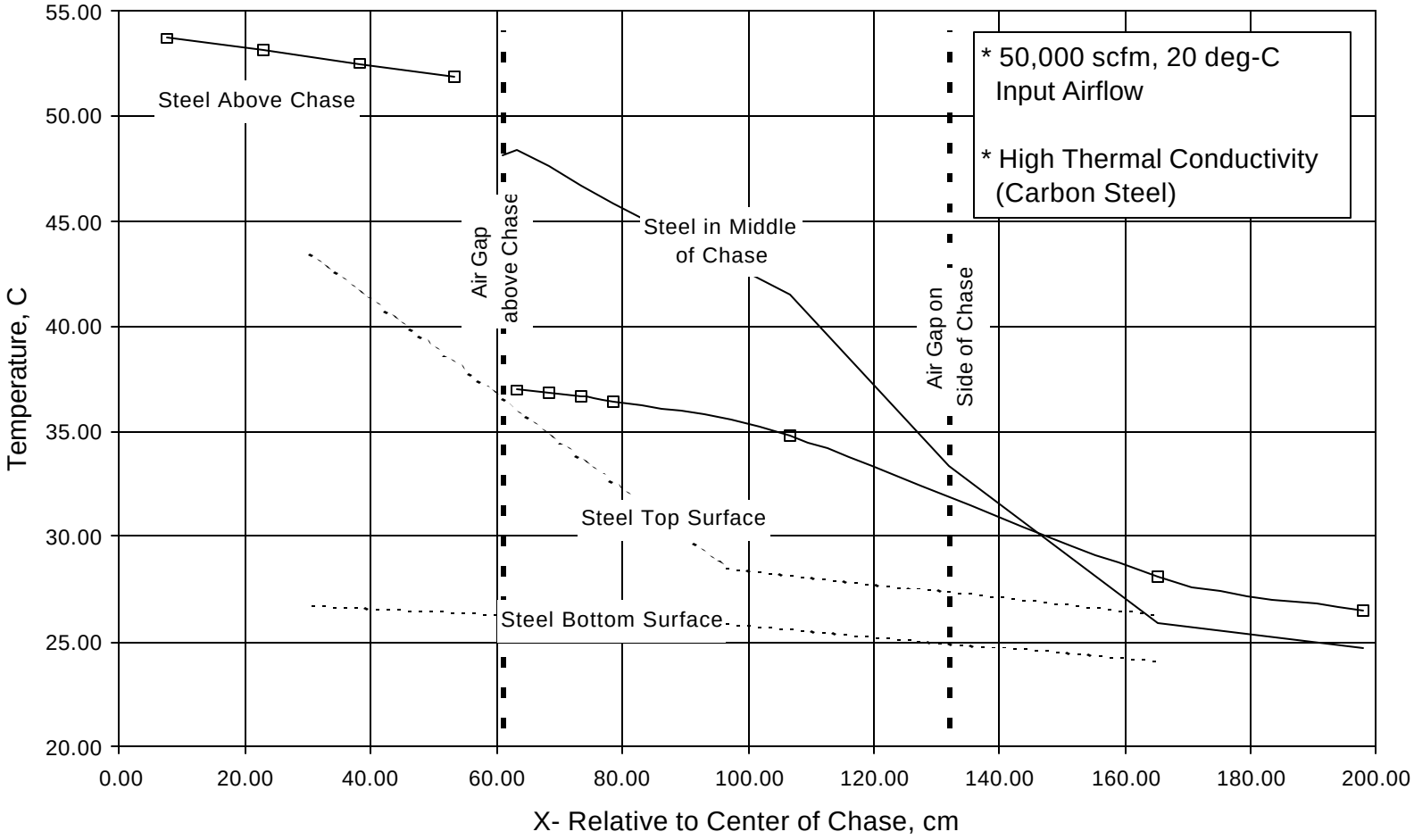

Fig. 9 Computed X-Dependence of Z-Peak (450 cm) Temperatures
50% of Airflow on Top

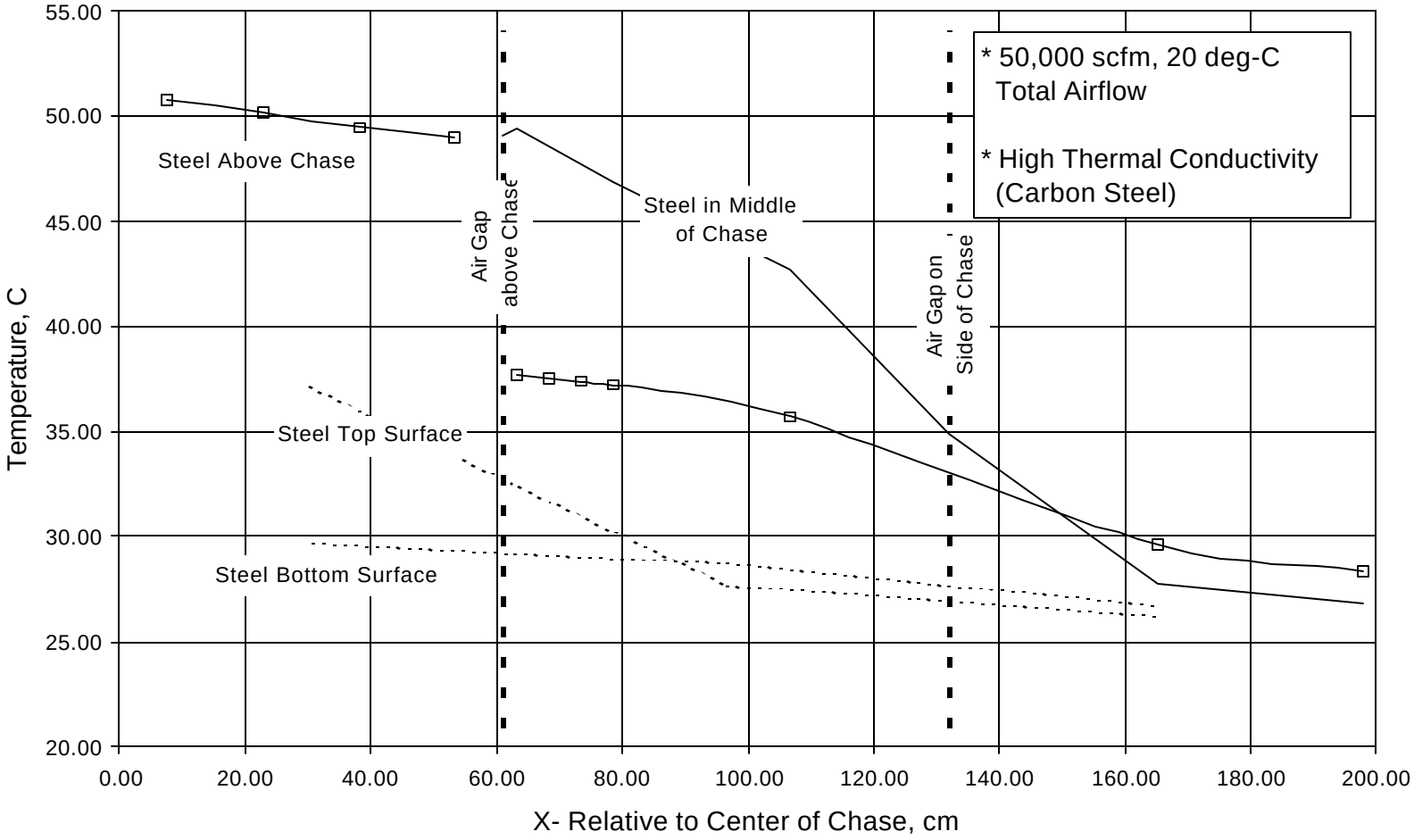

Fig. 10 Computed Y-Dependence of Z-Peak (450 cm) Temperatures
(Stagnant Air Above Shielding)

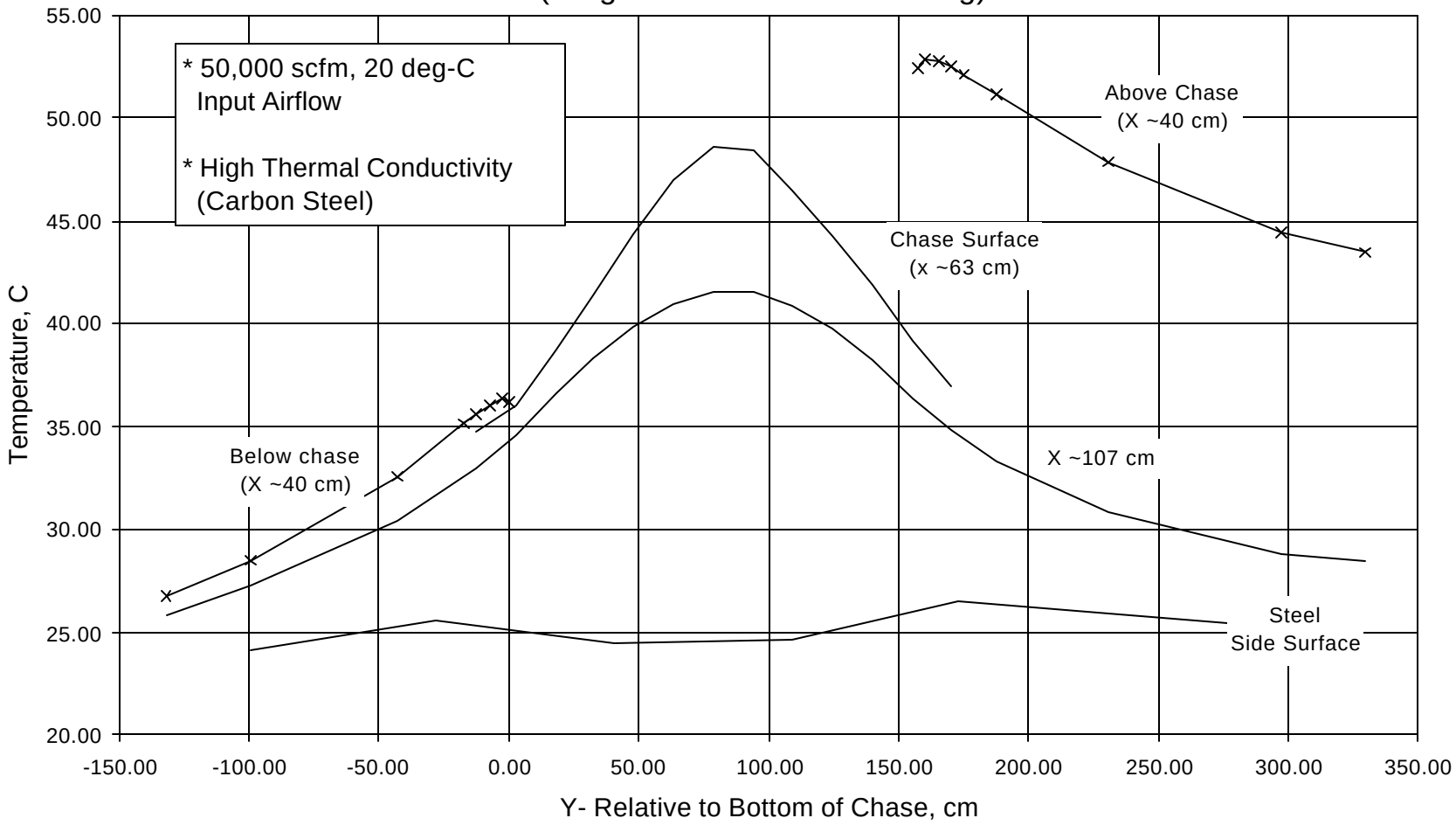

Fig. 11 Computed Y-Dependence of Z-Peak (450 cm) Temperatures
50% of Airflow on Top

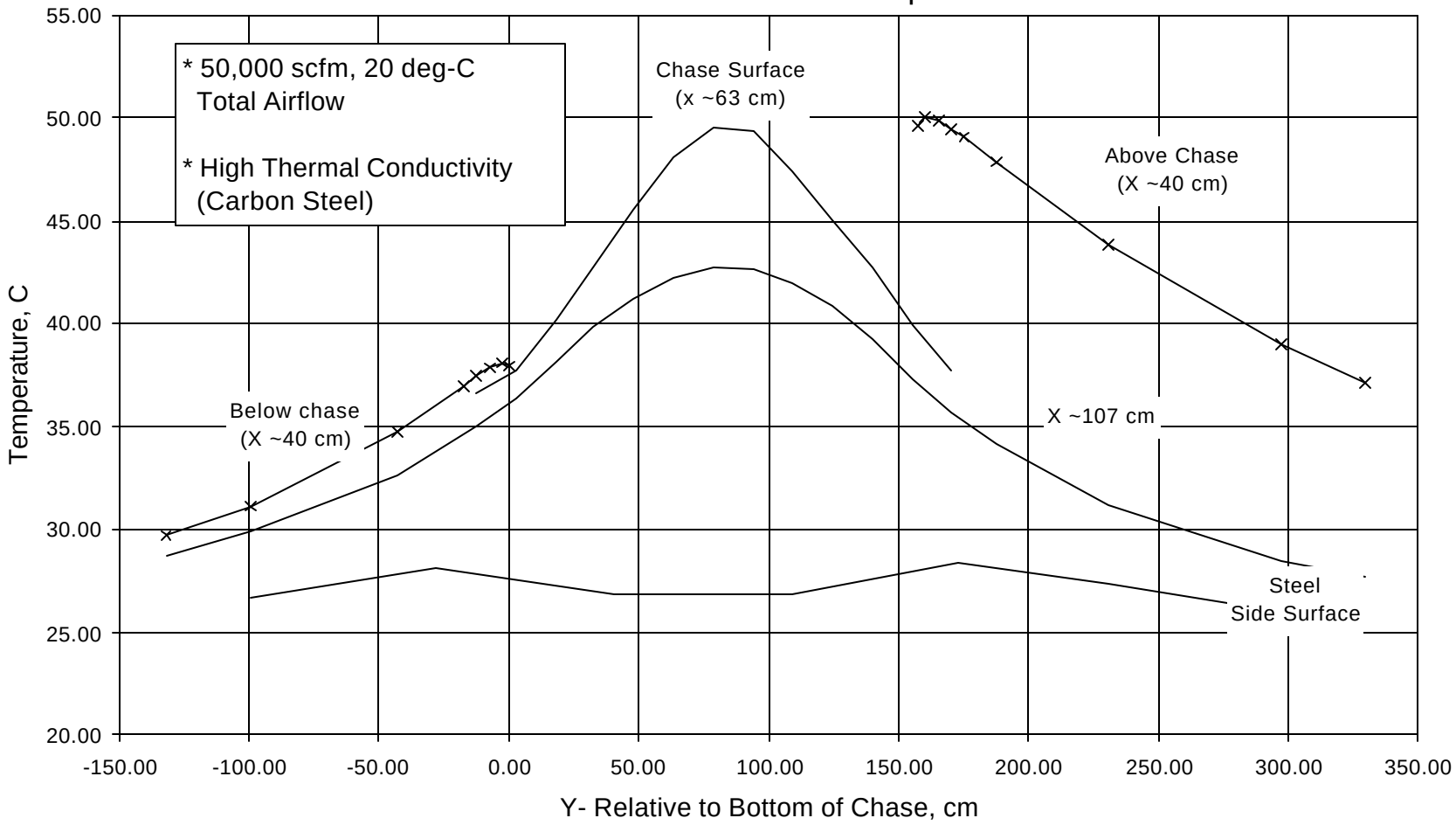

Fig. 12 Computed Heat Removal by Location Versus Air Flowrate
(Stagnant Air Above Shielding)

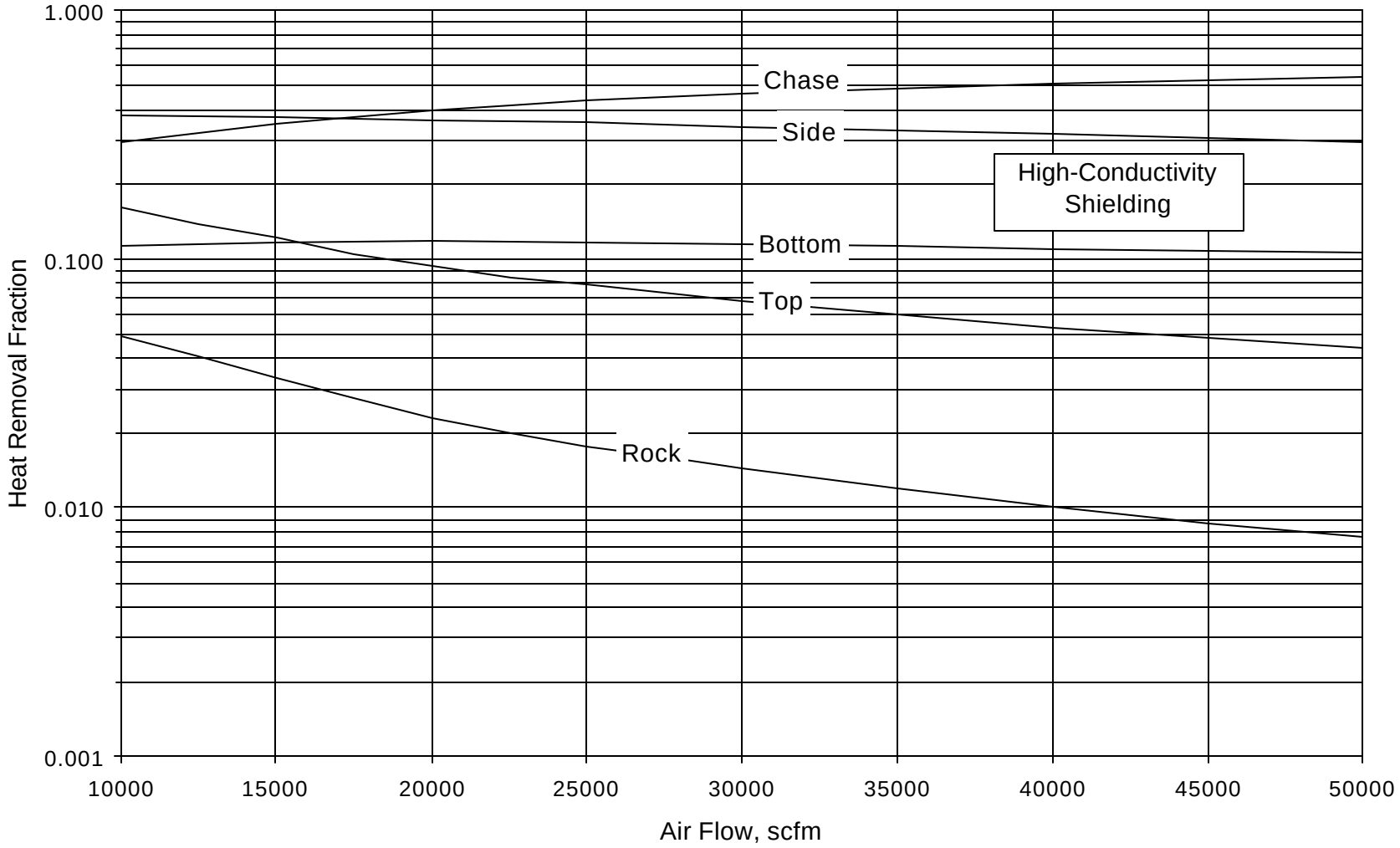

Fig. 13 Computed Heat Removal Capability Versus Division of Airflow

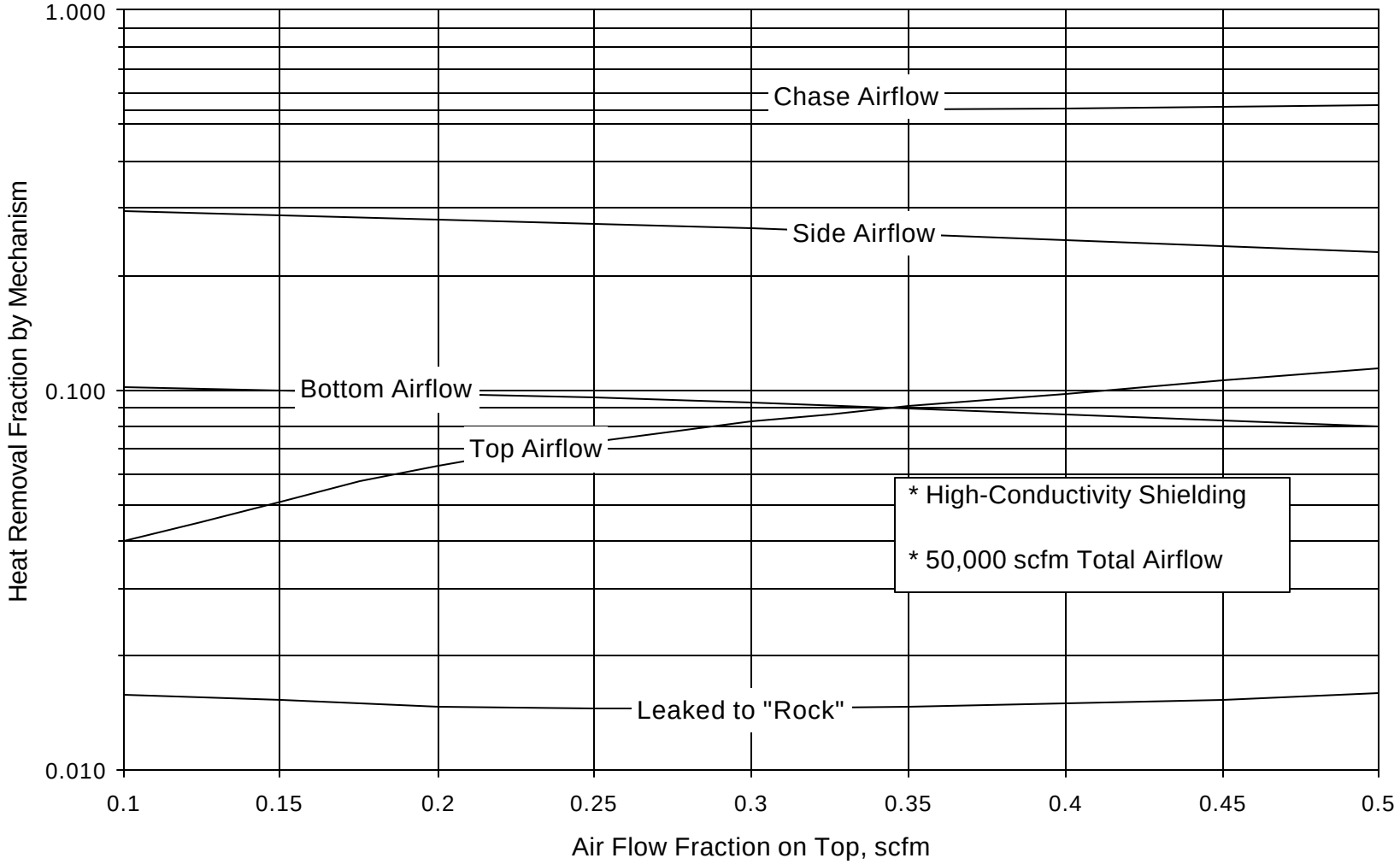

Fig. 14 Computed Shielding Temperatures Down the Chase
(Stagnant Air Above Shielding)

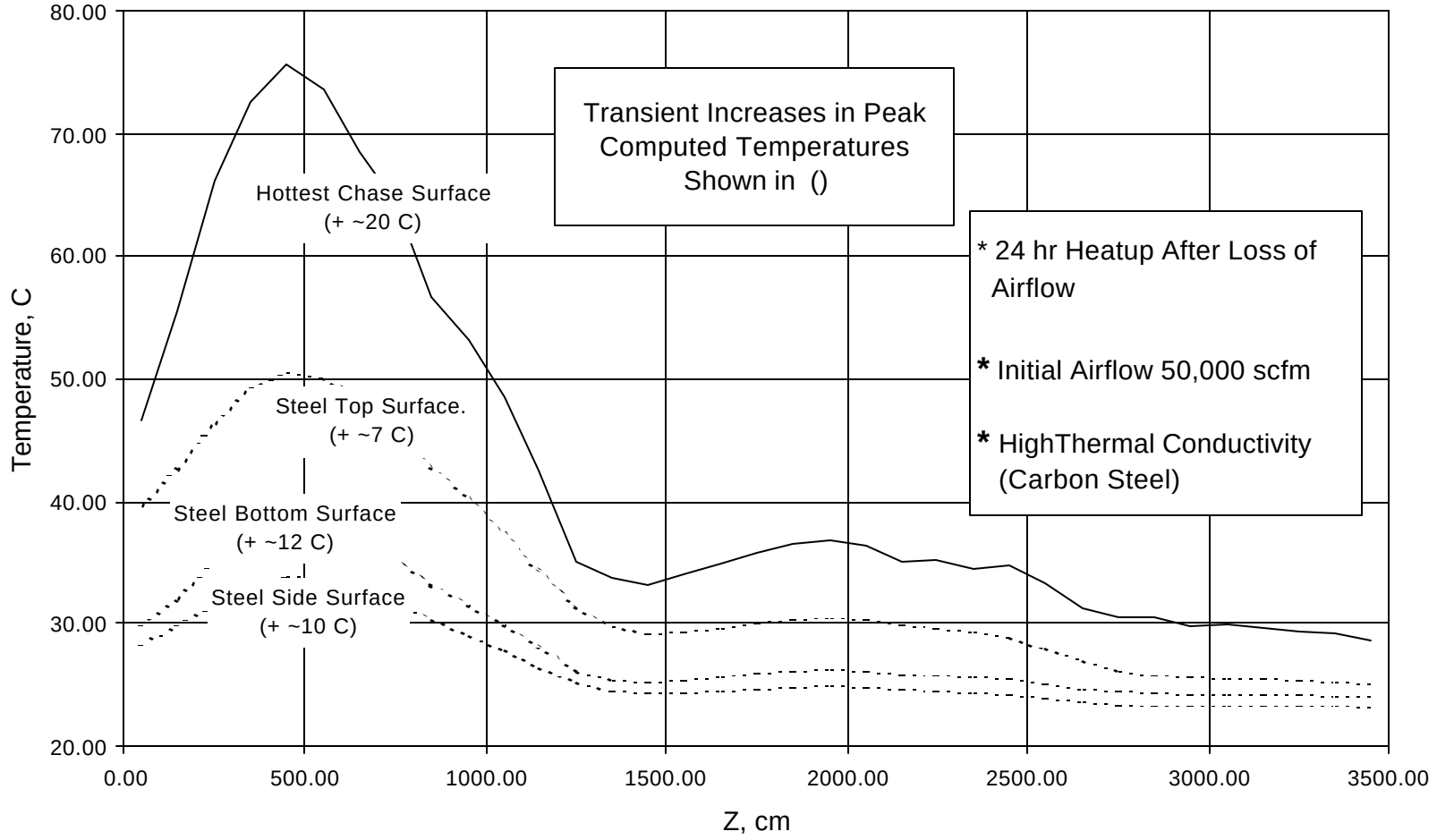

Fig. 15 Computed Air and ConcreteTemperatures Down the Chase
(Stagnant Air Above Shielding)

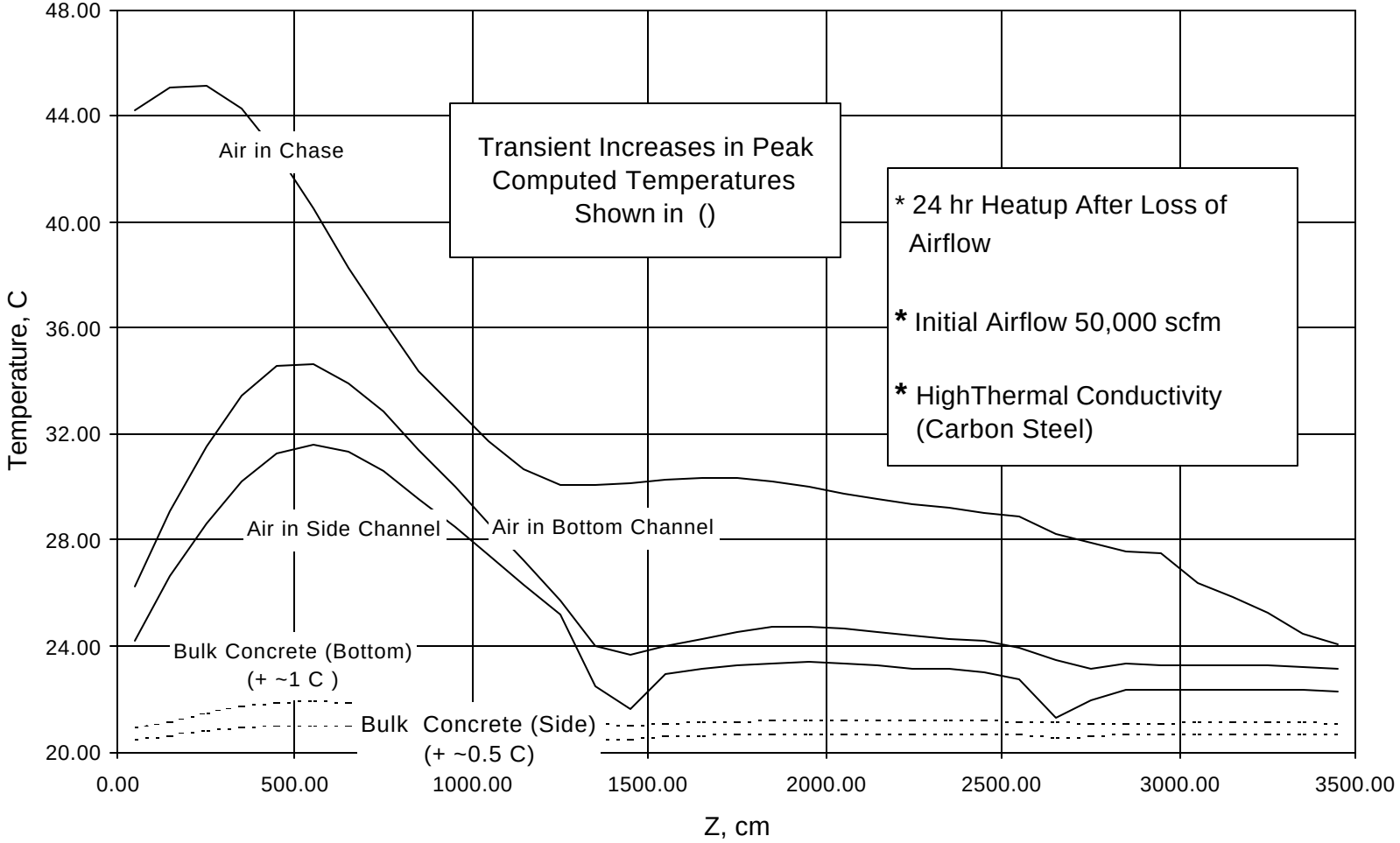

Appendix A- List and Contents of Archived Files

1. Contents of Archive NuMi_energy.zip

Includes original MARS Monte Carlo results supplied by FNAL plus analyses needed to (1) extrapolate to regions above and below chase and (2) construct SINDA/G input dataset

JobA.xls- first 13 m of chase plus generation and "validation" of extrapolation model

JobB.xls- next 11 m of chase

JobC.xls- final 11 m of chase

2. Contents of archive: NuMi_res.zip

Principal results in graphical form

Numi_sum.xls- Contains (1) scoping, (2) hydraulic, and (3) power distribution analyses.

NuMi3.xls- Contains model cross sections and results for cases with stagnant air on top of the steel shielding.

Plotted heat flow distributions include cases:
Carbon steel Conductivity, 10,000-50,000 scfm flow
Stainless steel Conductivity, 10,000-50,000 scfm flow
Carbon steel Conductivity, 10,000-50,000 scfm flow, 50% higher power

Plotted temperature profiles include cases:
Carbon steel Conductivity, 50,000 scfm flow
Carbon steel Conductivity, 10,000 scfm flow
Carbon steel Conductivity, 50,000 scfm flow
Stainless steel Conductivity, 50,000 scfm flow
Sudden LOF from 50,000 scfm, carbon steel Conductivity
Steady-state after LOF(10 scfm), carbon steel Conductivity
Carbon steel Conductivity, 50,000 scfm flow, 50% higher power

NuMi4.xls- Contains model cross sections and results for cases with forced air on top of the steel shielding.

Plotted heat flow distributions include cases:

Carbon steel Conductivity, 10,000-50,000 scfm flow

Plotted temperature profiles include cases:
Carbon steel Conductivity, 50,000 scfm flow, 10% on top
Carbon steel Conductivity, 50,000 scfm flow, 50% on top

3. Contents of archive: numi_sinda.zip

SINDA/G input source listings and output. All files in this archive are in unix text format.

SINDA/G input decks:
numi3.sin runs cases with stagnant air on top of the steel shielding
numi3lc.sin runs cases with stagnant air and stainless steel conductivity
numi4.sin runs cases with flowing air on top of the steel shielding

SINDA/G Output files:
numi3.ss- stagnant air on top, carbon steel conductivity, 10,000-50,000 scfm flow, steady-state
numi3lc.ss- stagnant air on top, stainless steel conductivity, 10,000-50,000 scfm flow, steady-state
numi4.ss- flowing air on top, carbon steel conductivity, 10,000-50,000 scfm flow, steady-state
numi3_150.ss- stagnant air on top, carbon steel conductivity, 10,000-50,000 scfm flow, steady-state, 50% higher power
numi3_150.ss- stagnant air on top, carbon steel conductivity, 10,000-50,000 scfm flow, steady-state, 50% higher power
numi3.loftr- stagnant air on top, sudden LOF from 50,000 scfm, carbon steel conductivity, transient
numi3.lofss- stagnant air on top, sudden LOF from 50,000 scfm, carbon steel conductivity, steady-state